



UPPSALA
UNIVERSITET

DiVA 

<http://uu.diva-portal.org>

This is an author produced version of a paper published in *Physical Review B*. This paper has been peer-reviewed but does not include the final publisher proof-corrections or journal pagination.

Citation for the published paper:

Kapaklis, Vassilios et al

"Violation of Hund's third rule in structurally disordered ferromagnets"

Physical Review B, 2011, Vol. 84, Issue 2, article 024411]

URL: <http://dx.doi.org/10.1103/PhysRevB.84.024411>

Access to the published version may require subscription.

Published with permission from: American Physical Society



Violation of Hund's third rule in structurally disordered ferromagnets

V. Kapaklis,* P. T. Korelis, and B. Hjörvarsson

Department of Physics and Astronomy, Uppsala University, Box 516, SE-75120, Uppsala, Sweden

A. Vlachos, I. Galanakis, and P. Pouloupoulos

Department of Materials Science, School of Natural Sciences, University of Patras, 26504 Patras, Greece

K. Özdoğan

Department of Physics, Yildiz Technical University, 34210 Istanbul, Turkey

M. Angelakeris

Department of Physics, Aristotle University of Thessaloniki, 54124 Thessaloniki, Greece

F. Wilhelm and A. Rogalev

European Synchrotron Radiation Facility (ESRF), B.P.220, 38043 Grenoble, France

Violation of Hund's third rule caused by structural disorder is observed for the induced magnetic moment of Zr, using X-ray magnetic circular dichroism. The induced spin and orbital magnetic moments are anti-parallel in the crystalline state, but parallel in an amorphous state of the investigated Co- and Fe-based materials. First principles calculations are used to provide physical insight into the dependency of the spin-orbit coupling on the interatomic distance and coordination number.

PACS numbers: 75.30.Cr, 71.70.Ej, 71.20.-b

Keywords: Magnetic susceptibility, Spin-orbit coupling, Electron density of states and band structure

I. INTRODUCTION

Hund's rules are generally viewed as highly successful empirical laws describing the electronic structure of multi-electron atoms¹. Reports on violations of Hund's third rule are rare, with few exceptions found in literature. Hund's third rule states that elements having less-than-half-filled electronic shells, should have their spin and orbital moments anti-parallel aligned. The opposite should be valid for more-than-half-filled electronic shells. The first report on the violation of Hund's third rule was made by Hjelm *et al.*², describing the electronic structure of Uranium, using first principle calculations. Subsequent theoretical efforts revealed possible violations in intermetallic compounds³⁻⁵. Experimental observations of this effect were initially reported by Wilhelm *et al.*⁶ for W, and by Herrero-Albillos *et al.*⁷ for Co. The work on W triggered a vivid discussion on the influence of the structure and chemical environment on the induced orbital moment, arising from the spin-orbit coupling^{8,9}, a discussion which is still far from being settled. X-ray magnetic circular dichroism (XMCD) can be used to determine, with element specificity, the spin and orbital contributions to the moment. Even very small magnetic moments, such as obtained in Au for the case of multilayers, nanoparticles and intermetallic alloys, can be measured with high precision¹⁰⁻¹². Thus, XMCD is highly suitable to obtain information on the validity of Hund's third rule.

In this article we discuss the influence of structural disorder in transition metal alloys on the electronic configuration. We use Zr containing alloys as a prototype

for these studies and XMCD to probe the induced magnetic moment of Zr. We compare the spin and orbital contribution to the moment in crystalline and disordered Zr containing layers, in which the bond length and coordination number are vastly different. The presence of disorder has previously been demonstrated to give rise to decreased contribution to the orbital moment in Fe in amorphous FeCoZr layers, while the orbital moment of Co is retained¹³. Thus structural disorder gives rise to a number of intricate magnetic properties¹³⁻¹⁶.

II. EXPERIMENTAL DETAILS

Amorphous Fe₉₁Zr₉ and Co₉₅Zr₅ films, with thickness of 5000 and 4000 Å, respectively, were deposited on Si (001) wafers by direct current magnetron sputtering at room temperature¹⁷. The alloy compositions were determined by Rutherford Back Scattering spectrometry. Two crystalline CoZrPt alloy thin films, with a total film thickness of 2500 Å, were deposited on polyimide substrates in a multisource e-beam evaporation system at room temperature. Energy Dispersive X-ray Spectroscopy measurements were used to determine their compositions (Co₈₃Zr₁₀Pt₇ and Co₈₆Zr₁₀Pt₄).

Ferromagnetic Resonance (FMR) experiments, were carried out at 8.5 GHz, using the X-ray detected magnetic resonance (XDMR) dedicated spectrometer¹⁸. In Fig. 1 the FMR linewidth ΔH of the amorphous Co₉₅Zr₅ film can be compared to the one of the polycrystalline Co₈₆Zr₁₀Pt₄ film. The width of the resonance is substantially broader for the polycrystalline film ($\Delta H \sim 30$ mT)

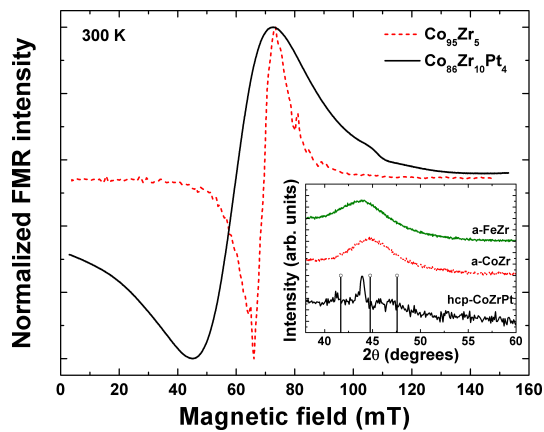


FIG. 1. FMR spectra for the amorphous $\text{Co}_{95}\text{Zr}_5$ and crystalline $\text{Co}_{86}\text{Zr}_{10}\text{Pt}_4$ thin films. The very small width of the FMR linewidths is an indication of the high degree of structural and magnetic homogeneity for the amorphous film. The inset shows X-ray diffraction patterns from amorphous $\text{Co}_{95}\text{Zr}_5$, $\text{Fe}_{91}\text{Zr}_9$ and crystalline $\text{Co}_{86}\text{Zr}_{10}\text{Pt}_4$ thin films. The vertical lines represent diffraction from reference hcp-*Co* powder.

as compared to the one of the amorphous film ($\Delta H \sim 6$ mT). The very narrow ΔH in the amorphous film is consistent with a very high degree of structural and magnetic homogeneity¹⁹. Structural analysis of the $\text{Fe}_{91}\text{Zr}_9$ and $\text{Co}_{95}\text{Zr}_5$ films was performed using Grazing Incidence X-ray diffraction (GI-XRD), and with $\theta - 2\theta$ XRD for the CoZrPt films. In both cases, $\text{Cu K}\alpha$ radiation (1.5418 Å) was used as a source. A broad halo, characteristic for amorphous materials, was recorded from the $\text{Fe}_{91}\text{Zr}_9$ and $\text{Co}_{95}\text{Zr}_5$ samples (inset of Fig. 1). The CoZrPt samples, on the other hand, exhibit narrow diffraction peaks, consistent with a textured polycrystalline structure. Comparing the diffraction pattern from a reference polycrystalline hcp *Co* powder to our experimental peaks in Fig. 1, we observe that the film peaks are shifted to lower angles. This shift originates from an enlarged cell volume and reveals larger interatomic distances in the CoZrPt film as compared to pure hcp *Co*. All samples exhibit in-plane magnetization.

The XMCD measurements were carried out on the beamline ID12 at the European Synchrotron Radiation Facility (ESRF) in Grenoble, France²⁰. The X-ray absorption spectrum (XAS) at both the Zr $L_{3,2}$ and Pt $L_{3,2}$ edges were measured using the total fluorescence yield (TFY) detection mode and in a backscattering geometry. The applied magnetic field, up to 1 T, was produced by a superconducting cryomagnet and was applied at 15 degrees grazing incidence with respect to the film surface. This field was adequate to saturate magnetically the samples. The XMCD measurements on the $\text{Fe}_{91}\text{Zr}_9$ sample were performed at 10 K, well below the magnetic ordering temperature of 190 K. The ordering temperature of the Co-based samples is much higher, which allowed us

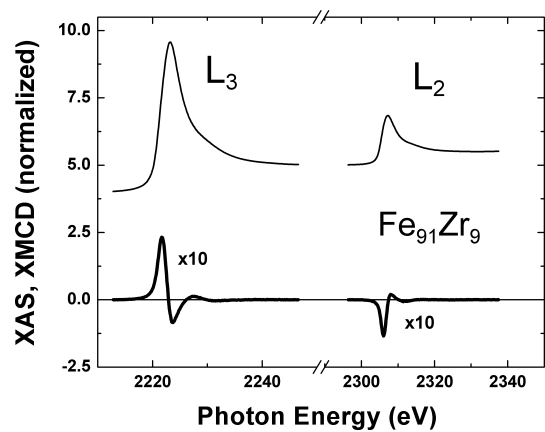


FIG. 2. XAS and XMCD spectra at the Zr L-edges obtained from the amorphous $\text{Fe}_{91}\text{Zr}_9$ film. A clear XMCD signal proves the existence of an induced magnetic moment in Zr. Compared to the XAS, the XMCD signal is rather small, therefore it is multiplied by a factor of 10 for clarity.

to perform the XMCD measurements on these samples at 300 K.

The X-ray source for the Zr L-edges is a HELIOS-II type helical undulator. At the energies of the Zr L_3 (~ 2.22 keV) and Zr L_2 edges (~ 2.31 keV), the Bragg angle of the double Si(111) crystal monochromator is below the Brewster angle; therefore the degree of circular polarization of the monochromatic beam is reduced to 64 % and 46 %, respectively. The X-ray source for the Pt L-edges (above 11 keV) was an Apple-II-type helical undulator. At this energy, the degree of circular polarization of the monochromatic beam is over 95 %. The XMCD spectra were obtained as the difference between consecutive XAS scans recorded with opposite helicities of the incoming circularly polarized X-ray beam. To ensure that the measured XMCD spectra are free of any experimental artifact, the data were collected for both directions of the external applied magnetic field (parallel and antiparallel to the incoming X-ray beam). The TFY mode is the easiest method to use in the presence of a magnetic field; nevertheless, self-absorption corrections to the measured fluorescence spectrum in the case of Zr L-edges are required to obtain the absorption coefficient. As the film thickness is comparable to the penetration depth of the X-rays at the Zr L-edges, the XAS spectra had to be corrected for self-absorption effects, which are responsible for the white line saturation effects^{21,22}.

Using the same experimental procedure as described previously²³, the absorption spectra after corrections for the partial X-ray circular polarization, were corrected for self-absorption effects, taking into account the chemical composition, density, thickness of the film, angle of incidence of the X-ray beam, and finally the solid angle of the detector. The Zr edge-jump intensity ratio L_2/L_3 was then normalized to 1:2 according to the statistical edge jump ratio (defined as the ratio between the oc-

Sample	μ_L/μ_S	μ_S (μ_B/atom)	μ_L (μ_B/atom)
Zr moments			
Fe ₉₁ Zr ₉ (a)	0.070	-0.15	-0.010
Co ₉₅ Zr ₅ (a)	0.025	-0.12	-0.0030
Co ₈₆ Zr ₁₀ Pt ₄ (c)	-0.11	-0.080	0.0091
Co ₈₃ Zr ₁₀ Pt ₇ (c)	-0.14	-0.068	0.0097
Pt moments			
Co ₈₆ Zr ₁₀ Pt ₄ (c)	0.18	0.40	0.075
Co ₈₃ Zr ₁₀ Pt ₇ (c)	0.16	0.37	0.061

TABLE I. Experimental magnetic moments for Zr and Pt in Zr-based alloy thin films. The error bars in the analysis are approximately $\pm 10\%$ ²⁶. (a): amorphous, (c): crystalline. The spin magnetic moments in the Table are effective spin moments determined, within the uncertainty of a magnetic dipole term T_z . However, for highly isotropic systems, such as cubic, polycrystalline or amorphous, this term is negligible²⁷.

cupation numbers for the two spin-orbit-split core levels $j = 1/2$ and $3/2$). This L_2/L_3 value is well-established for 4d transition metals²⁴. Moreover, this statistical Zr edge-jump intensity ratio L_2/L_3 is very close to 2.01 tabulated in tables by McMaster *et al.*²⁵. Transmission experiments, which could be an alternative route and where no corrections are needed, are impossible for the samples investigated here, since the growth restrictions (such as substrates and buffer layers) are not compatible with standard transmission substrates¹⁷.

III. RESULTS AND DISCUSSION

The XAS and the corresponding XMCD spectra, recorded at the Zr $L_{3,2}$ -edges for the amorphous Fe₉₁Zr₉ film, are presented in Fig. 2. Similar results were also recorded for all the CoZr films. The existence of XMCD signals at the Zr L- edges reveals the presence of an induced magnetic moment in Zr. To our knowledge, this is the first demonstration of an induced moment in Zr. Knowing the direction of the magnetic field and the helicity of the beam, we can determine the Zr moment to be anti-parallel to the Fe or Co magnetic moment. This behavior is consistent with Zr belonging to the beginning of the 4d transition elements, having small occupancy of the 4d band. XMCD spectra recorded at the Zr $L_{3,2}$ -edges for the amorphous Co₉₅Zr₅ and polycrystalline Co₈₆Zr₁₀Pt₄ films are presented in Fig. 3. The more intense XMCD signal from the Co₉₅Zr₅ film indicates larger induced moment in Zr as compared to Zr in Co₈₆Zr₁₀Pt₄.

We applied the sum-rule analysis on the XAS and XMCD results, to determine the spin and orbital contributions to the magnetic moment of Zr^{28,29}. For the white line intensities, one has to subtract the continuum from the XAS. When the white line intensities are large, as for the case of Zr in this work (Fig. 2) the continuum is represented by a step function⁶. For the case of Pt, where

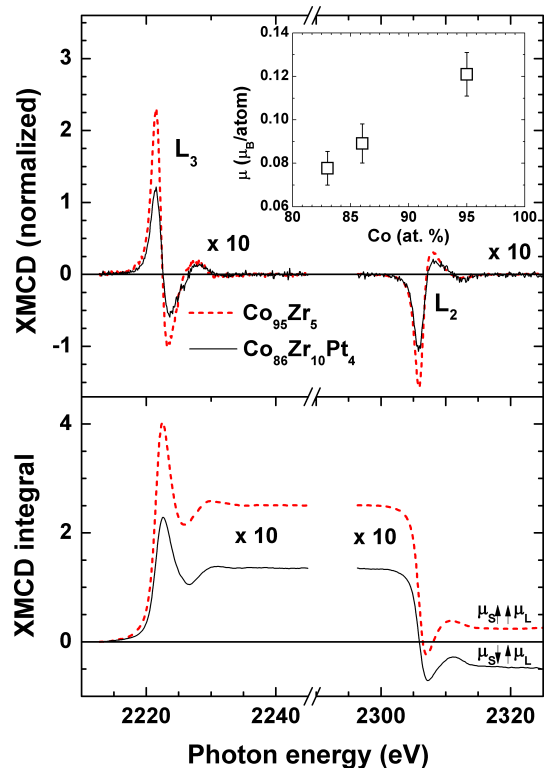


FIG. 3. XMCD spectra recorded at the Zr L-edges for the crystalline Co₈₆Zr₁₀Pt₄ and the amorphous Co₉₅Zr₅ thin films. In the inset, the absolute value of the induced magnetic moment of Zr is plotted as a function of the Co at. % concentration. The change in relative orientation of μ_L and μ_S is clearly visible in the XMCD integrals below.

the white line intensities are small, this approach can not be applied. Taking into account that Pt in our samples is in a hcp lattice, we have followed the analysis which is described in detail in Ref.³⁰ for hcp Pt. The results are summarized in Table I. In the Co containing samples, the total induced magnetic moment is found to scale with the Co concentration, regardless of the structural order (inset of Fig. 3). The largest value of the induced Zr moment ($\sim 0.16 \mu_B/\text{atom}$) is obtained for the Fe₉₁Zr₉ sample. Thus, the effective polarization of Zr appears to be dependent on the source of the polarization. The induced magnetic moments for Pt in the polycrystalline films are also given in the table. The magnitude of the Pt magnetic moments and the μ_L/μ_S ratios, are comparable to the ones of CoCrPt alloys with hcp symmetry^{30,31}.

The relative orientation of the Zr spin and orbital magnetic moments are also listed in Table I. For the crystalline samples, μ_L and μ_S are anti-parallel, as expected from Hund's third rule for materials with less-than-half-filled 4d shell. In the amorphous samples, μ_L and μ_S are parallel, as shown by the XMCD signal integrals, in the lower part of Fig. 3. These results, clearly prove the change in relative orientation of μ_L and μ_S upon disorder. Only few experimental verifications of

this effect are found in the literature^{6,7} and all are restricted to crystalline samples. Furthermore, the theoretical predictions for VAu_4 , MnAu_4 and VPt_3 ordered alloys^{3,4} have been principally attributed to spin-orbit interactions and the interplay between interatomic and intra-atomic interactions. In the case of W in Fe/W multilayers⁶, W is towards the middle of the 5*d* series and a small charge transfer from Fe to W could be responsible for this behavior. A violation of Hund's third rule for an element in the beginning of the 4*d* series, like Zr, is therefore not perceivable within that conceptual framework.

We performed first principle calculations in order to obtain a better understanding of the underlying mechanism. For this purpose, the full-potential localized-orbital method (FPLO)³² and local-spin-density approximation (LSDA)³³ was used. When using the FPLO approach, disordered alloys can be treated within the coherent potential approximation (CPA)³⁴. However, CPA is only used in conjunction with the scalar-relativistic approximation, which does not allow for the calculation of the orbital moment. We therefore decided to use ordered alloys as a benchmark for the distance dependence of the magnetic induction. CoZr is known to crystallize in the bcc-like CsCl structure. When the stoichiometry is kept to 1:1 the alloy is not magnetic but the inclusion of Co impurities at antisites induces ferromagnetic order³⁵. Thus, a unit cell double the size of CsCl was used, with three Co and one Zr atoms per cell, and a varying lattice constant between 2.46 and 3.06 Å, with a step of 0.05 Å. The distance between Co and Zr atoms was kept at $\sqrt{3}/2$ of the lattice constant. We applied the Dirac formulation to account for relativistic effects and a $20 \times 20 \times 10$ *k*-mesh. The equilibrium lattice constant for Co_3Zr was found to be 2.95 Å, in-between the values for the pure elements (2.74 Å for bcc Co and 3.49 Å for bcc Zr). In all cases, convergence to a magnetic solution was obtained; the Co atoms have their spin magnetic moments pointing parallel while Zr atoms exhibit an induced spin magnetic moment antiparallel to that of the Co atoms. As shown in Fig. 4, around the equilibrium lattice constant the μ_L/μ_S ratio for Zr is negative, in agreement with Hund's third rule, but below 2.66 Å, it changes sign. The corresponding calculations for bcc Fe_3Zr show similar behavior and the change of the sign of the μ_L/μ_S ratio for Zr occurs for a lattice constant of 2.50 Å. When changing the coordination number in Co_3Zr , from 8 (bcc) to 12 (hcp), the Zr μ_L/μ_S ratio maintained a negative value for all the examined lattice constants.

The violation of the third Hund's rule has been explained in the case of VAu_4 , using perturbation theory, as a result of the effect of ligand states³. It was shown that the spin-orbit coupling of the Au atoms influences, through the hybridization of the *d*-orbitals, the orbital moment at the V site and is actually causing its reversal. Thus, it is within reason to argue that in a similar way, Co(Fe) spin-orbit coupling can influence the Zr orbital moment, leading to its reversal, since hybridization be-

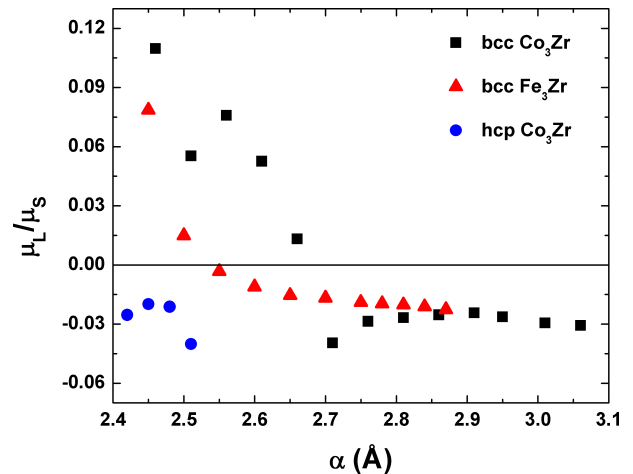


FIG. 4. First principle calculations of the induced μ_L/μ_S ratio for Zr as a function of the lattice parameter α for various crystallographic structures, as indicated.

tween *d*-states at Co(Fe) and Zr sites is strong enough to induce a spin magnetic moment at the Zr site. Hybridization effects would be more important for the amorphous films, since the concentration of Zr is smaller with respect to the theoretically studied compounds. Our calculated results also show that the influence of the Co(Fe) spin-orbit coupling depends on the interatomic distance and the coordination number, which is expected, since the latter influences the strength of the hybridization between the *d*-orbitals at different sites. Finally, we should mention that in first principle calculations, even in the Dirac formulation, the use of LSDA accounts actually only for contributions to the orbital moment arising from the spin moments, via the spin-orbit coupling and this consistently results to an underestimation of its absolute value with respect to experiments. The latter explains the finding that the sign reversal for the μ_L/μ_S ratio occurs for a lattice constant significantly smaller than the equilibrium one. Physical meaning should be attributed mainly to the observed trend and not the actual value of the lattice constant for which the reversal occurs.

The results of the calculations clearly indicate that a sign reversal of μ_L can occur when the interatomic distance between Co(Fe) and Zr is decreased. For the hcp polycrystalline CoZrPt samples, all interatomic distances are larger than that of Co-Co. Therefore, violation of the third Hund's rule should not be expected in that case. For the amorphous samples, the mean distances between dissimilar atoms (Co-Zr) can be smaller than that of Co-Co³⁶. This has been recently demonstrated by extended X-ray absorption fine structure measurements and molecular dynamics calculations, which compared crystalline and amorphous NiZr alloys of the same concentration³⁷. Chemical short-range order appeared^{37,38} and the significant decrease of the bond length between dissimilar atoms was accompanied by a drastic decrease of the coor-

dination number. Both effects are in favor of sign reversal for μ_L , according to our calculations.

IV. CONCLUSIONS

The violation of Hund's third rule for an element in the beginning of the $4d$ series gives a new perspective to the unsettled discussion on the interplay between the induced orbital moment and spin-orbit coupling^{8,9}. The interatomic distance and coordination number can have a strong effect on the relative orientation of the spin and orbital magnetic moments. Thus, the root of the changes in magnetic properties upon amorphization can be understood, and in principle be calculated. Further develop-

ment of both theoretical concepts and methodology as well as experimental techniques³⁸ addressing the fundamental properties of disordered materials will certainly provide further insight and understanding of these new and unique phenomena.

V. ACKNOWLEDGEMENTS

We thank the E.S.R.F. for the excellent operating conditions. The work was supported by the Swedish Research Council, The Knut and Alice Wallenberg Foundation and the Research Committee of the University of Patras, under Grant Karatheodori 2009, Nr. C905.

-
- * Corresponding author.
- ¹ C. Kittel, *Introduction to Solid State Physics*, 8th ed. (John Wiley & Sons, 2005).
 - ² A. Hjelm, O. Eriksson, and B. Johansson, *Phys. Rev. Lett.*, **71**, 1459 (1993).
 - ³ I. Galanakis, P. M. Oppeneer, P. Ravindran, L. Nordström, P. James, M. Alouani, H. Dreyse, and O. Eriksson, *Phys. Rev. B*, **63**, 172405 (2001).
 - ⁴ I. Galanakis, M. Alouani, P. M. Oppeneer, H. Dreyssé, and O. Eriksson, *J. Phys.: Condens. Matter*, **13**, 4553 (2001).
 - ⁵ P. M. Oppeneer, I. Galanakis, A. Grechnev, and O. Eriksson, *J. Magn. Magn. Mater.*, **240**, 371 (2002).
 - ⁶ F. Wilhelm, P. Pouloupoulos, H. Wende, A. Scherz, K. Baberschke, M. Angelakeris, N. K. Flevaris, and A. Rogalev, *Phys. Rev. Lett.*, **87**, 207202 (2001).
 - ⁷ J. Herrero-Albillos, L. M. García, F. Bartolomé, and A. T. Young, *EPL (Europhysics Letters)*, **93**, 17006 (2011).
 - ⁸ R. Tyer, G. van der Laan, W. M. Temmerman, and Z. Szotek, *Phys. Rev. Lett.*, **90**, 129701 (2003).
 - ⁹ F. Wilhelm, P. Pouloupoulos, H. Wende, A. Scherz, K. Baberschke, M. Angelakeris, N. K. Flevaris, and A. Rogalev, *Phys. Rev. Lett.*, **90**, 129702 (2003).
 - ¹⁰ F. Wilhelm, M. Angelakeris, N. Jaouen, P. Pouloupoulos, E. T. Papaioannou, C. Mueller, P. Fumagalli, A. Rogalev, and N. K. Flevaris, *Phys. Rev. B*, **69**, 220404 (2004).
 - ¹¹ Y. Yamamoto, T. Miura, M. Suzuki, N. Kawamura, H. Miyagawa, T. Nakamura, K. Kobayashi, T. Teranishi, and H. Hori, *Phys. Rev. Lett.*, **93**, 116801 (2004).
 - ¹² F. Wilhelm, P. Pouloupoulos, V. Kapaklis, J.-P. Kappler, N. Jaouen, A. Rogalev, A. N. Yaresko, and C. Politis, *Phys. Rev. B*, **77**, 224414 (2008).
 - ¹³ T. Hase, H. Raanaei, H. Lidbaum, C. Sánchez-Hanke, S. Wilkins, K. Leifer, and B. Hjörvarsson, *Phys. Rev. B*, **80**, 134402 (2009).
 - ¹⁴ L. Gao, X. Jiang, S.-H. Yang, P. M. Rice, T. Topuria, and S. S. P. Parkin, *Phys. Rev. Lett.*, **102**, 247205 (2009).
 - ¹⁵ A. T. Hindmarch, C. J. Kinane, M. MacKenzie, J. N. Chapman, M. Henini, D. Taylor, D. A. Arena, J. Dvornak, B. J. Hickey, and C. H. Marrows, *Phys. Rev. Lett.*, **100**, 117201 (2008).
 - ¹⁶ P. Pouloupoulos, V. Kapaklis, P. E. Jonsson, E. T. Papaioannou, A. Delimitis, S. D. Pappas, D. Trachylis, and C. Politis, *Appl. Phys. Lett.*, **96**, 202503 (2010).
 - ¹⁷ P. T. Korelis, A. Liebig, M. Björck, B. Hjörvarsson, H. Lindbaum, K. Leifer, and A. R. Wildes, *Thin Solid Films*, **519**, 404 (2010).
 - ¹⁸ J. Goulon, A. Rogalev, F. Wilhelm, G. Goujon, C. Brouder, A. Yaresko, J. Ben Youssef, and M. V. Indenbom, *J. Magn. Magn. Mater.*, **322**, 2308 (2010).
 - ¹⁹ W. Platow, A. N. Anisimov, G. L. Dunifer, M. Farle, and K. Baberschke, *Phys. Rev. B*, **58**, 5611 (1998).
 - ²⁰ A. Rogalev, J. Goulon, C. Goulon-Ginet, and C. Malgrange, in *Magnetism and Synchrotron Radiation*, Lecture Notes in Physics, Vol. 565, edited by E. Beaupaire, J. Kappler, G. Krill, and F. Scheurer (Springer Berlin / Heidelberg, 2001) pp. 60–86.
 - ²¹ L. Tröger, D. Arvanitis, K. Baberschke, H. Michaelis, U. Grimm, and E. Zschech, *Phys. Rev. B*, **46**, 3283 (1992).
 - ²² R. Nakajima, J. Stöhr, and Y. U. Idzerda, *Phys. Rev. B*, **59**, 6421 (1999).
 - ²³ F. Wilhelm, N. Jaouen, A. Rogalev, W. G. Stirling, R. Springell, S. W. Zochowski, A. M. Beesley, S. D. Brown, M. F. Thomas, G. H. Lander, S. Langridge, R. C. C. Ward, and M. R. Wells, *Phys. Rev. B*, **76**, 024425 (2007).
 - ²⁴ T. K. Sham, *Phys. Rev. B*, **31**, 1888 (1985).
 - ²⁵ <http://www.csrri.iit.edu/mucal.html> and references therein.
 - ²⁶ This error bar refers to the determination of the absolute moment value for μ_S and μ_L . The error bar for the μ_L/μ_S is significantly lower, since asymmetry factors as low as 2×10^{-4} are detectable on the specific beamline.
 - ²⁷ R. Wu and A. J. Freeman, *Phys. Rev. Lett.*, **73**, 1994 (1994).
 - ²⁸ B. T. Thole, P. Carra, F. Sette, and G. van der Laan, *Phys. Rev. Lett.*, **68**, 1943 (1992).
 - ²⁹ P. Carra, B. T. Thole, M. Altarelli, and X. Wang, *Phys. Rev. Lett.*, **70**, 694 (1993).
 - ³⁰ P. Pouloupoulos, *Int. J. Mod. Phys. B*, **19**, 4517 (2005).
 - ³¹ P. Pouloupoulos, F. Wilhelm, V. Kapaklis, N. Jaouen, N. Angelakeris, A. Rogalev, and C. Politis, *Phys. Status Solidi A*, **201**, 3243 (2004).
 - ³² K. Koepf and H. Eschrig, *Phys. Rev. B*, **59**, 1743 (1999).
 - ³³ J. P. Perdew and Y. Wang, *Phys. Rev. B*, **46**, 12947 (1992).
 - ³⁴ K. Koepf, B. Velický, R. Hayn, and H. Eschrig, *Phys. Rev. B*, **58**, 6944 (1998).

- ³⁵ G. Zhu and H. Bakker, *Physica B*, **211**, 134 (1995).
- ³⁶ Y. Babanov, A. Sidorenko, A. Ryazhkin, V. Shvetsov, J. Moessinger, and H. Kronmueller, *Nucl. Instrum. Meth. A*, **405**, 400 (1998).
- ³⁷ X. Liu, X. D. Hui, H. Y. Hou, T. Liu, and G. L. Chen, *Phys. Lett. A*, **372**, 3313 (2008).
- ³⁸ A. Hirata, P. Gua, T. Fujita, Y. Hirotsu, A. Inoue, A. R. Yavari, T. Sakurai, and M. Chen, *Nature Materials*, **10**, 28 (2011).